Mansour *et al. Int J Concr Struct Mater* (2024) 18:82
https://doi.org/10.1186/s40069-024-00716-6

International Journal of Concrete Structures and Materials

RESEARCH Open Access

# Numerical Response of Concrete-Filled Steel Tubular (CFST) Columns Externally Strengthened with FRP Composites Subjected to Cyclic Loading

Walid Mansour[1,2*], Bothaina Osama[3], Weiwen Li[1*], Peng Wang[1,4] and Md. Habibur Rahman Sobuz[5]

**Abstract**

The ultimate load-carrying capacity of concrete-filled steel tubular (CFST) columns exposed to monotonic loadings can be greatly increased by strengthening those columns, and the occurrence of the steel tube's outward buckling can be postponed. The current research aims to study the possibility of improving the structural characteristics of CFST columns exposed to cyclic loadings in terms of lateral load capacity and absorbed energy by strengthening them with different patterns of fiber-reinforced polymer (FRP) sheets. The ABAQUS software was used to create a three-dimensional (3D) non-linear finite element model (FEM) to simulate the behavior of FRP-strengthened CFST columns exposed to monotonic and cyclic loadings. After ascertaining the accuracy of the proposed model's results in successfully predicting failure patterns and lateral loads compared to the experimental results of tested specimens available in the literature, the model was used to create a parametric study. The parametric study focused on the impacts of the thickness, location, and length of the strengthening sheets on the failure pattern, lateral load-carrying capacity, stiffness, cumulative energy, absorbed energy, and viscous damping factor of the CFST columns exposed to cyclic loadings. The results revealed that the un-strengthened specimen displayed a maximum lateral load of 185 kN and a viscous damping factor of 45.2% at a lateral drift of 5.7%. On the other hand, strengthening the CFST column using five layers of FRP sheets exhibited the highest lateral load of all investigated columns (50% more than the un-strengthened specimen). Additionally, at a lateral drift of 5.7%, the decrease in viscous damping factor of CFST specimens due to strengthening using 1, 2, 3, 4, and 5 layers of FRP sheets with respect to the control specimen was 7.9%, 14.9%, 20.8%, 27.7%, and 30.3%, respectively.

**Keywords** Concrete-filled steel tubular (CFST) columns, Cyclic loading, Finite element model, Fiber-reinforced polymers (FRPs), Absorbed energy, Stiffness, Viscous damping

Journal information: ISSN 1976-0485 / eISSN 2234-1315.

*Correspondence:
Walid Mansour
waled_mansour@eng.kfs.edu.eg
Weiwen Li
liweiwen@szu.edu.cn
Full list of author information is available at the end of the article

## 1 Introduction

Composite columns are currently widely recognized in the construction industry, particularly in high-rise buildings, due to their ease of fabrication (Han & Beijing., 2007; Wang et al., 2023), enhanced seismic performance (Dong et al., 2022; Elchalakani & Zhao, 2008), and larger deformability (Wang et al., 2004). Due to the benefits of combining steel and concrete, concrete-filled steel tubular (CFST) columns are increasingly being used in many modern projects (Madenci et al., 2022; Mansour & Fayed, 2021; Serras et al., 2016). Steel has strong tensile strength and ductility, while concrete exhibits excellent compressive strength and stiffness (Hatzigeorgiou & Beskos, 2005). On the one hand, core concrete plays an important role in preventing the inward local buckling of the steel tube, while the confinement of the concrete is enhanced by the steel tube (Chin et al., 2019; Wang et al., 2022). On the other hand, the outward buckling of the steel tube negatively affects the efficiency and ultimate load-carrying capacity of such composite columns.

Recent experimental and numerical studies have focused on delaying the emergence of the steel tube's outward buckling in order to improve the structural performance of CFST columns, whether through internal reinforcing or external strengthening. Spiral-confined reinforced concrete-filled steel tubular (SCRCFST) columns have recently been presented as a new type of CFST column. Extensive investigations were conducted to study the influence of the amount and properties of spiral reinforcements, the confined concrete area, the internal stiffeners, and the spacing of the spiral reinforcements on the behavior of short SCRCFST columns subjected to axial compression (Ahmed et al., 2021; Chen et al., 2021; Ding et al., 2014, 2016; Hu et al., 2020; Yuan et al., 2022). The results revealed that as the volumetric ratio or yield strength of the spiral reinforcements increased, the ultimate capacity and ductility of the SCRCFST columns remarkably improved. Furthermore, utilizing smaller spiral reinforcement spacing in addition to a significant longitudinal reinforcement ratio could improve the axial load of SCRCFST columns.

The use of fiber-reinforced polymer (FRP) sheets is one of the methods presented during the last decade to resist corrosion, improve durability, and avoid or delay the early outward local buckling of steel tubes (Hu & Seracino, 2014; Li et al., 2020). Wang et al. (2020) experimentally evaluated the ultimate axial bearing capacity of carbon fiber-reinforced polymer (CFRP) confined steel tube confined concrete (STCC) subjected to monotonic axial compressive loading. The main studied parameters were the number of layers of CFRP wrap, the width-to-thickness ratio of steel tube, and the sectional corner radius. The test results showed that the outward local buckling of the steel tube was delayed by using CFRP wrapping, which effectively constrains the deformation of the steel tube. Moreover, the ultimate capacity and ductility of core concrete were improved because of the confinement from both steel tube and CFRP sheets. The findings of the Fang et al. (2019) and Xu et al. (2020) experiments are consistent with previous findings that FRP can improve the capacity of strengthened CFST columns regardless of fiber type (glass or carbon). According to Zhang et al. (2023), the axial compressive load of CFST columns was increased by 64.2% after being wrapped by four layers of FRP sheets relative to the un-strengthened specimen. In contrast, when only one strengthening layer was used, the improvement ratio was only 28.7%.

The FRP material demonstrated a high ability to improve the ultimate load capacity and ductility of CFST columns exposed to axial compressive loads. As a result, experimental and numerical studies were expected to be concerned with the behavior of the externally FRP-strengthened CFST columns and exposed to cyclic loadings. However, many researchers were interested in studying the behavior of CFST columns exposed to cyclic loadings (Brown et al., 2015; Dong et al., 2022; Elchalakani & Zhao, 2008; Han & Yang, 2005; Qian et al., 2014; Skalomenos et al., 2014; Varma et al., 2002), while the behavior of FRP-strengthened CFST columns subjected to cyclic loadings is rarely studied in the literature. Herein lies the importance of the current study. Yuan et al. (2018) conducted an experimental study to investigate the performance of circular CFST columns exposed to both cyclic loading and an acid rain attack. It was concluded that corrosion decreases the yield strength, ductility, ultimate capacity, and dissipation energy of the CFST columns. Additionally, experimental and numerical investigations revealed that the local buckling of steel tube at a lateral drift of 4% decreased the strength of CFST under cyclic loading (Cao et al., 2021; Patel et al., 2014). The seismic performance of CFST columns is little affected by the shear studs welded on the steel tube (Liu et al., 2018), while CFST columns with circular cross-sections were more resistant to the outward buckling of the steel tube than those with square cross-sections (Ji et al., 2023).

According to the findings of investigations on the behavior of CFST columns subjected to cyclic loadings, the majority of these columns failed due to the outward buckling of steel tubes, which led to strength degradation (Hu et al., 2022, 2024; Xu et al., 2023; Zhou & Liu, 2010). Therefore, it is essential to avoid or even postpone the outward local buckling of steel tubes in order to increase the maximum lateral load, absorbed energy, and stiffness of CFST columns subjected to cyclic loadings. Few researchers used the FRP sheets to wrap the

CFST columns subjected to several cycles of unloading and reloading in the axial direction (cyclic axial compression) in an effort to improve their maximum capacity and ductility. The results showed that the test specimens subjected to cyclic axial compression all failed due to explosive rupture of the FRP wrap in the mid-height region (Yu et al., 2014). On the contrary, to the authors' best knowledge, the response of FRP-strengthened CFST columns subjected to cyclic loadings in the lateral direction has not been reported in the available literature.

From the above-mentioned introduction, this paper intends to numerically investigate the cyclic response of CFST columns externally wrapped using FRP sheets. It is expected that the high mechanical characteristics of the FRP sheets may lead to a favorable failure pattern as the outward local buckling of the steel tube will be prevented or even delayed. In order to accomplish research objectives with a scientific manner, a three-dimensional (3D) non-linear finite element model (FEM) was initially created using the finite element analysis tool ABAQUS (ABAQUS, 2017). Then the accuracy of the proposed numerical model was ascertained in two phases. The first phase was using the results of previous studies on FRP-strengthened CFST columns subjected to monotonic loadings to confirm the validity of the defined materials, such as confined concrete, steel tube, and FRP sheets. In the second step, it was ascertained that the numerical model could successfully predict the failure patterns and the hysteresis responses by comparing its results with the experimental results of un-strengthened CFST columns exposed to cyclic loadings available in the literature. The developed FEM was utilized to carry out a parametric investigation after it was confirmed that the model accurately represented the cyclic response of FRP-strengthened CFST columns. The variables studied were the impacts of FRP thickness, FRP location, and effective length of the FRP sheets on failure patterns, lateral load–drift responses, initial stiffness, cumulative energy, absorbed energy, and the viscous damping factor of strengthened CFST columns subjected to cyclic loadings.

## 2 Finite Element Modeling

Using the commercial finite element (FE) simulation software ABAQUS (ABAQUS, 2017), a three-dimensional (3D) solid non-linear FE model was constructed to simulate the response of the CFST columns externally strengthened using CFRP sheets subjected to cyclic loading.

### 2.1 Element Types and Meshes

To mimic the core concrete, 8-node linear brick elements (C3D8R) were adopted, while 4-node doubly curved thin shell elements (S4R) were used to simulate both steel tubes and FRP sheets. The effectiveness of the suggested model and the necessary computational time are both greatly impacted by the identification of the element type for each individual member of CFST columns strengthened with FRP. Additionally, setting the appropriate mesh size solves convergence issues that prevent the model from being completed and guarantees effective load transmission. In the current model, the mesh size was set to approximately 1/15 of the diameter of the CFST tube column based on the recommendations of Tao et al. (2013), Mansour et al., (2022). The details of the elements, mesh size, and boundary conditions are depicted in Fig. 1.

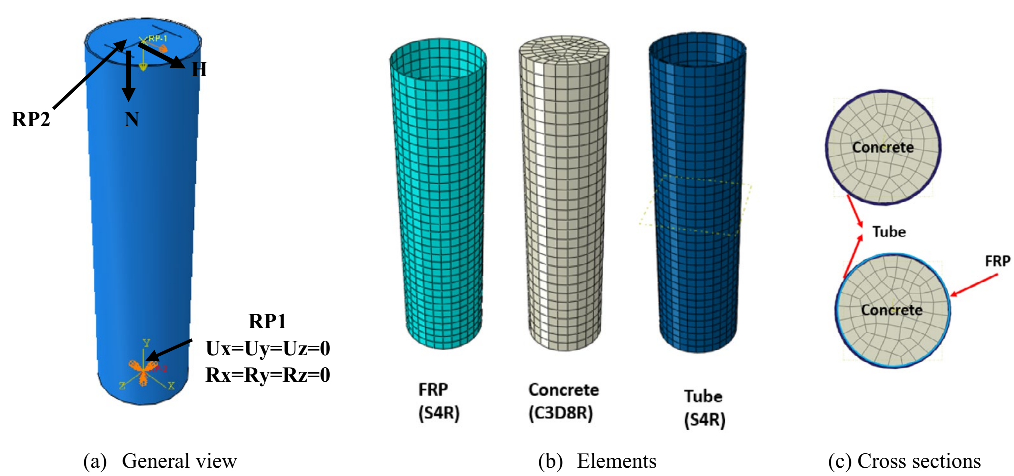


**Fig. 1** Elements, mesh size, and boundary condition of the FE model

### 2.2 Modeling of Interactions, Loading and Boundary Conditions

The interactions between the inner surface of steel tubes and the outer surface of concrete were simulated using the surface-to-surface contact model provided by ABAQUS. Within this model, a hard contact relationship was considered for the normal interaction to allow for full transfer of compression forces and to prevent transmission of tensile stresses across the contact. Additionally, in accordance with the suggestions of Tao et al. (2013), Tam et al., (2023), Mansour et al., (2024), the Coulomb friction formulation was used to account for the tangential interaction with a friction coefficient of 0.6. No debonding between the strengthening FRP sheets and the steel tubes was observed in experiments. Consequently, the adhesive surface was represented between them using the perfect bond model (tie interaction), where the steel surface and FRP were selected to be the master and host surfaces, respectively. Furthermore, two coupling interactions were utilized to attach support and loading reference points RP1 and RP2, respectively, to the lower and upper surfaces of the CFST column, as shown in Fig. 1a. The lower reference point's (RP1) degrees of freedom were all restricted along the $X$, $Y$, and $Z$ axes to simulate the fixed support. At the upper reference point (RP2), the cyclic loading (H) protocol shown in Fig. 2 was applied at the $X$-direction in addition to the constant axial compression load (N) at the $Y$-direction simulated by the force-controlled loading model. Both axial and cyclic loadings were applied using the static general step available in ABAQUS.

### 2.3 Material Modeling

#### *2.3.1 Confined Concrete*

In concrete-filled steel tubes externally strengthened with FRP composites, the concrete infill should be simulated as confined concrete because the concrete is constrained by both the steel tube and the FRP. The confined stress–strain curve was simulated using the approach suggested in Tao et al. (2013), Tao et al., (2011). Three zones should be established, as shown in Fig. 3, in order to successfully describe the real response of the confined concrete. The first zone is a linear elastic stage that represents the elastic stress range (from point O to point A). In the elastic stage, the concrete modulus of elasticity $E_c$ and Poisson's ratio $\upsilon$ should be defined. The $E_c$ was estimated using Eq. (1) based on the recommendation of ACI (ACI, 2008), whereas the $\upsilon$ was considered to be 0.20 (Abdal et al., 2023; Basha et al., 2023; Elwakkad et al., 2023; Tao et al., 2013):

$$E_c = 4700\sqrt{\bar{f}_c}, \tag{1}$$

where $\bar{f}_c$ is the compressive cylinder strength of concrete (in MPa).

Furthermore, in the first zone, effect of the steel and FRP wrap's constraints on the concrete response were not taken into account, and the stress–strain of the core concrete was comparable to that of unconfined concrete. Consequently, the model offered by Samani and Attard (2012) (Eq. 2) is implemented to define the ascending curve OA:

$$\frac{\sigma}{\bar{f}_c} = \frac{AX + BX^2}{1 + (A-2)X + (B+1)X^2} \; 0 < \varepsilon < \varepsilon_{co}, \tag{2}$$

where $X = \frac{\varepsilon}{\varepsilon_{co}}$, $A = \frac{E_c \varepsilon_{co}}{\bar{f}_c}$, and $B = \frac{(A-1)^2}{0.55} - 1$, $\sigma$ is the compressive stress corresponding to compressive strain ($\varepsilon$), $\varepsilon_{co}$ represents the peak strain of concrete under uniaxial compression, determined by Eq. (3) according to Nicolo et al. (1994):

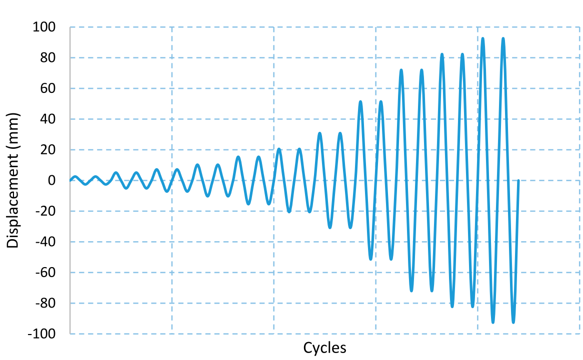


**Fig. 2** Protocol of cyclic loading

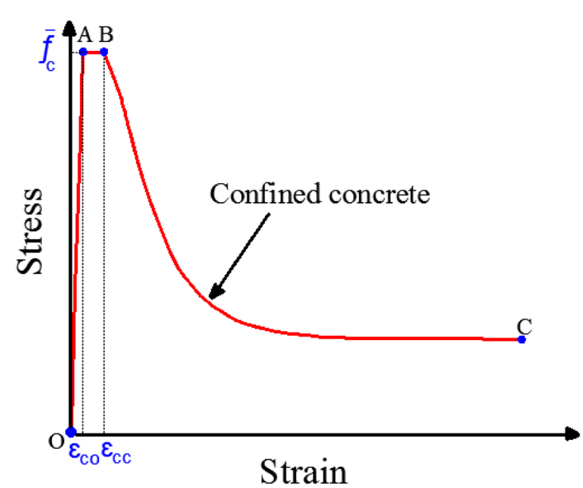


**Fig. 3** Confined concrete modeling

$$\varepsilon_{co} = 0.00076 + \sqrt{\left(0.626\bar{f}_c - 4.33\right) \mathrm{x}\ 10^{-7}}. \quad (3)$$

After reaching the peak compressive stress $\left(\bar{f}_c\right)$ at point A, the plateau stage (AB), the second zone, will be initiated. The plateau zone defines the plastic progress of the core concrete after reaching peak stress. Then, the strain continues to increase until the core concrete's lateral expansion was stopped by steel tube and FRP sheets. At point (B), the strain is calculated using Eq. (4) as suggested by Samani and Attard (2012):

$$\frac{\varepsilon_{cc}}{\varepsilon_{co}} = e^K, K = (2.9224 - 0.00376\bar{f}_c)\left(\frac{f_B}{\bar{f}_c}\right)^{0.3124+0.002\bar{f}_c}, \quad (4)$$

where $f_B$ is the confining stress of the core concrete at point $B$ caused by the FRP wraps and the steel tube. Tao et al. (2013) proposed Eq. (5) to determine the confining stress of the core concrete ($f_B$):

$$f_B = \frac{(1 + 0.027f_y)e^{-0.02\frac{D}{t}}}{1 + 1.6e^{-10}(\bar{f}_c)^{4.8}}. \quad (5)$$

Beyond Point B, the compressive stress–strain response of the core concrete exhibited softening behavior, the third zone BC, as depicted in Fig. 3. The stress–strain curve at the third zone is described using the exponential function suggested by Binici (2005) as listed in Eq. (6):

$$\sigma = f_r + \left(\bar{f}_c - f_r\right)\exp\left[-\left(\frac{\varepsilon - \varepsilon_{co}}{\alpha}\right)^{\beta}\right]\varepsilon > \varepsilon_{cc}, \quad (6)$$

where $f_r$ stands for the residual stress, $\alpha$ and $\beta$ are parameters defining the descending part of the third zone (BC).

According to Tao et al. (2013), $\beta$ is equal to 1.2, whereas the values of $f_r$, $\alpha$, and $\xi_c$ were estimated using Eqs. (7), (8) and (9), respectively:

$$f_r = 0.7\left(1 - e^{-1.38\xi_c}\right)\bar{f}_c \le 0.25\bar{f}_c, \quad (7)$$

$$\alpha = 0.04 - \frac{0.036}{1 + e^{6.08\xi_c - 3.49}}, \quad (8)$$

$$\xi_c = \left(f_{FRP}A_{FRP} + f_{ys}A_s\right)/\bar{f}_cA_c, \quad (9)$$

where $\xi_c$ is the confinement factor, $f_{FRP}$ and $A_{FRP}$ are the tensile strength and cross-sectional area of the FRP, $f_{ys}$ and $A_s$ are the yield strength and cross-sectional area of the steel tube, and $A_c$ is the cross-sectional area of concrete.

In ABAQUS, the concrete damage plasticity (CDP) model was adopted to express the characteristics of the confined concrete. The required parameters used to construct the CDP model are defined in Table 1. Furthermore, the fracture energy method was used to describe the tensile behavior of the confined concrete. Following this criterion, the fracture energy ($G_f$) and the corresponding tensile strength ($f_t$) of concrete were defined using Eq. (10) (Tang et al., 2020) and Eq. (11) (ACI, 2008), respectively:

**Table 1** Concrete damage plasticity parameters

| Dilation angle | Eccentricity | Bi-axial to uniaxial compressive stress | Shape factor | Viscosity parameter |
|---|---|---|---|---|
| 40 | 0.1 | 1.277 | 0.667 | 0.0005 |

$$G_f = 2.5\left(10^{-3}\right)\alpha\left(0.10\bar{f}_c\right)^{0.70}, \quad (10)$$

$$f_t = 0.33\sqrt{\bar{f}_c}, \quad (11)$$

where $\alpha = 1.25d_{\max} + 10$, and $d_{\max}$ is the diameter of coarse aggregate in the concrete.

### 2.4 Steel Tube

In the current FE model, the stress–strain behavior of steel tube and steel I-sections was simulated using the five segments shown in Eq. (12) and previously developed by Han (2007):

$$\sigma_s = \begin{cases} E_s\varepsilon_s & \varepsilon_s \le \varepsilon_e \\ -A\varepsilon_s^2 + B\varepsilon_s + c & \varepsilon_e < \varepsilon_s < \varepsilon_{e1} \\ f_{ys} & \varepsilon_{e1} < \varepsilon_s < \varepsilon_{e2} \\ f_{ys}\left[1 + 0.6\frac{\varepsilon_s - \varepsilon_{e2}}{\varepsilon_{e3} - \varepsilon_{e2}}\right] & \varepsilon_{e2} < \varepsilon_s < \varepsilon_{e3} \\ 1.6f_{ys} & \varepsilon_s < \varepsilon_{e3} \end{cases}, \quad (12)$$

where $f_{ys}$ and $E_s$ are the yield strength and modulus of elasticity for steel, respectively. Furthermore, the strains ($\varepsilon_e, \varepsilon_{e1}, \varepsilon_{e2}, \varepsilon_{e3},$) were correlated with each other by the following relationships: $\varepsilon_e = \frac{0.8f_y}{E_s}$,$\varepsilon_{e1} = 1.50\varepsilon_e$,$\varepsilon_{e2} = 10\varepsilon_{e1}$, and$\varepsilon_{e3} = 100\varepsilon_{e1}$. The values of other parameters ($A$, $B$, and $C$) were calculated according to Ji et al. (2023): $A = \frac{0.20f_y}{(\varepsilon_{e1} - \varepsilon_e)^2}$,$B = 2A\varepsilon_{e1}$, and $C = 0.8f_y + A\varepsilon_e^2 - B\varepsilon_e$.

#### *2.4.1 FRP*

FRP wraps were simulated in the current FE model as an orthotropic material. The high tensile strength in the longitudinal direction was considered, whereas the compressive strength was completely disregarded. Therefore, the LAMINA material model was used to define the elastic modulus, shear modulus, and Poisson's ratio of the FRP composites, according to experimental studies used

**Table 2** Damage evolution of the FRP composites

| Longitudinal tensile fracture energy (N mm/mm$^2$) | Longitudinal compressive fracture energy (N mm/mm$^2$) | Transverse tensile fracture energy (N mm/mm$^2$) | Transverse compressive fracture energy (N mm/mm$^2$) |
|---|---|---|---|
| 91.6 | 79.9 | 0.22 | 1.1 |

in the validation process. The failure mode of the FRP wraps observed in the previous experimental investigations was tensile rupture; as a result, it was necessary to set the damage behavior parameters in the FE model. The damage behavior of the FRP composites was accurately defined in terms of modulus of elasticity ($E_f$), tensile strength ($f_f$), and damage criteria. The strength in longitudinal and transversal directions of the FRP composites, according to the manufacturer, was modeled via the Hashin damage model, while the parameters of damage evolution in FRP materials are listed in Table 2 based on the guidelines of Hany et al. (2016), Shi et al., (2012).

### 2.5 Initial Imperfections

The performance of the steel column is considerably influenced by the initial buckling and residual stresses. Therefore, an appropriate buckling analysis model along the CFST columns with an adequate number of eigenvalues is needed in order to accurately estimate the cyclic performance of CFST columns externally strengthened with FRP. The linear perturbation buckle step was initially developed to simulate the initial geometric buckling in the current FE model for both monotonic and cyclic loadings. As proposed by Sharif et al. (2019), the suggestion for the number of eigenvalues was 8.

### 2.6 Model Validation

To the authors' best knowledge, experimental data that examine the behavior of CFST columns strengthened with FRP sheets under the effect of cyclic loading have been rarely studied in the literature. Therefore, the validation process of the suggested FE model was divided into two stages. In the first stage, it was determined whether the numerical model accurately predicted the behavior of the CFST columns that had been externally strengthened with FRP and exposed to monotonic loading. In the second stage, the proposed model's accuracy was evaluated using a simulation of the behavior of bare CFST columns (without external FRP strengthening) exposed to cyclic loading.

Composite column specimens previously tested under either monotonic loading by Tang et al. (2020), Wang et al. (2020), and Zhang et al. (2023) or cyclic loading by Ji et al. (2023) were used to check the accuracy of the proposed FE model. Dimensions of CFST columns as well as properties of unconfined concrete, steel tubes, and FRP are listed in Table 3, while Table 4 shows the comparison between experimental and numerical ultimate loads, maximum displacement, and failure patterns. The comparison that was made demonstrated that the proposed numerical model could accurately predict the behavior of experimentally tested specimens that had either been subjected to monotonic or cyclic loadings. The ratio between the ultimate finite element and experimental load ranged from 0.92 to 1.03 with an average, standard deviation, and coefficient of variation (COV) of 1.00, 0.032, and 3.2%, respectively. Additionally, there was a significant correlation between the experimental findings and the numerical results for axial displacements under monotonic loading or lateral displacements under cyclic loading. The standard deviation, coefficient of variation, and average ratio of the numerical to experimental displacements were 0.044, 4.3%, and 1.02, respectively. Furthermore, the average ratio of numerical-to-experimental stiffness, along with the standard deviation and coefficient of variation were 1.08, 0.064, and 5.9%, respectively.

The accuracy of the numerical model did not stop at the successful prediction of the maximum load value of specimens and displacements at failure but extended to the patterns of collapse as well. No matter what kind of collapse took place or where it took place, as shown in Fig. 4, the FE model accurately predicted the pattern of collapse corresponding to each experimentally tested specimen. The numerical model was able to predict the outward local buckling of un-strengthened CFST columns, whether it occurred in the upper third of specimens under monotonic loading or close to the fixed support for specimens under cyclic loading. The FRP rupture failure pattern was consistent across all of the CFST columns that had been externally strengthened with FRP sheets, and the numerical model was successful in predicting where the FRP sheets would be cut.

Fig. 5 reveals that the numerical model well estimated the numerical responses in terms of load–axial shortening and load–longitudinal strain for bare and FRP-strengthened CFST columns exposed to monotonic loading with respect to experimental findings. The numerical elastic zone, ultimate zone, and softening zone were fairly acceptable, as the maximum recorded coefficient of variation between the numerical and experimental findings was just 4.3%. Furthermore, the performance of the CFST columns subjected to cyclic loadings could be accurately predicted by the developed numerical model. The excellent agreement between experimental lateral load–displacement (hysteresis curves) and numerical results is displayed in Fig. 5c–f.

**Table 3** Configurations and mechanical characteristics of all specimens used in the validation

| References | Specimen ID | Diameter mm | Thickness mm | Length mm | FRP thickness, mm (No. of layers) | Axial load kN | Properties of concrete | | Properties of steel tube | | Properties of FRP | |
|---|---|---|---|---|---|---|---|---|---|---|---|---|
| | | | | | | | $\bar{f}_c$ MPa | $f_t$ MPa | $E_s$ GPa | $f_{ys}$ MPa | $E_f$ GPa | $f_f$ MPa |
| Tang et al. (2020) | F114×3–0-A | 114.8 | 3.04 | 402 | 0 (0) | – | 31 | 1.84 | 188.6 | 355 | – | – |
| | F114×3–1-A | 114.6 | 3.04 | 402 | 0.167 (1) | – | 31 | 1.84 | 188.6 | 355 | 243 | 2600 |
| Wang et al. (2020) | PC-A-1-2 | 150 | 1.0 | 450 | 0.334 (2) | – | 55.4 | 2.46 | 210 | 188 | 245 | 4077 |
| | RC-A-1-2 | 150 | 1.0 | 450 | 0.334 (2) | – | 55.4 | 2.46 | 210 | 188 | 245 | 4077 |
| Zhang et al. (2023) | C0CFST | 159 | 4.0 | 636 | 0 (0) | – | 32.4 | 1.88 | 200 | 466.5 | – | – |
| | C1CFST | 159 | 4.0 | 636 | 0.15 (1) | – | 32.4 | 1.88 | 200 | 466.5 | 269.4 | 3406 |
| | C3CFST | 159 | 4.0 | 636 | 0.45 (3) | – | 32.4 | 1.88 | 200 | 466.5 | 269.4 | 3406 |
| | C1-C-0 | 220 | 4.0 | 900 | – | 0 | 52.9 | 2.4 | 204 | 316.7 | – | – |
| Ji et al. (2023) | C1-C-2 | 220 | 4.0 | 900 | – | 597 | 52.9 | 2.4 | 204 | 316.7 | – | – |
| | C1-C-3 | 220 | 4.0 | 900 | – | 896 | 52.9 | 2.4 | 204 | 316.7 | – | – |
| | C1-C-4 | 220 | 4.0 | 900 | – | 1194 | 52.9 | 2.4 | 204 | 316.7 | – | – |

**Table 4** Comparison between experimental (EXP) and numerical (FE) results

| Specimen ID | Ultimate load (kN) | | | Maximum displacement (mm) | | | *Stiffness (kN/mm) | | | Failure pattern | |
|---|---|---|---|---|---|---|---|---|---|---|---|
| | EXP | FE | FE/EXP | EXP | FE | FE/EXP | EXP | FE | FE/EXP | EXP | FE |
| F114×3-0-A | 867 | 869 | 1.00 | 29.8 | 29.9 | 1.00 | 302 | 352 | 1.17 | Outward buckling | Outward buckling |
| F114×3-1-A | 892 | 902 | 1.01 | 29.9 | 33.1 | 1.10 | 216 | 236 | 1.09 | FRP rupture | FRP rupture |
| PC-A-1-2 | 1493 | 1491 | 0.99 | 5.4 | 5.5 | 1.04 | 335 | 358 | 1.07 | FRP rupture | FRP rupture |
| RC-A-1-2 | 1653 | 1700 | 1.03 | 8.2 | 8.1 | 0.98 | 367 | 380 | 1.04 | FRP rupture | FRP rupture |
| C0CFST | 1809 | 1838 | 1.02 | 61.2 | 63.6 | 1.04 | 137 | 141 | 1.03 | Outward buckling | Outward buckling |
| C1CFST | 2283 | 2347 | 1.03 | 24.8 | 24.7 | 0.99 | 294 | 317 | 1.08 | FRP rupture | FRP rupture |
| C3CFST | 3134 | 3168 | 1.02 | 22.6 | 22.3 | 0.98 | 312 | 328 | 1.05 | FRP rupture | FRP rupture |
| C1-C-0 | 184 | 185 | 1.00 | 45.7 | 47.3 | 1.04 | 27.7 | 30.3 | 1.09 | Local buckling | Local buckling |
| C1-C-2 | 178 | 183 | 1.03 | 46.2 | 48.4 | 1.05 | 18.5 | 19.0 | 1.03 | Local buckling | Local buckling |
| C1-C-3 | 171 | 176 | 1.03 | 40.9 | 41.6 | 1.02 | 30.7 | 32.4 | 1.06 | Local buckling | Local buckling |
| C1-C-4 | 125 | 115 | 0.92 | 25.5 | 23.9 | 0.94 | 15.7 | 19.4 | 1.24 | Local buckling | Local buckling |
| Average | | | 1.00 | | | 1.02 | | | 1.08 | | |
| Standard deviation | | | 0.032 | | | 0.044 | | | 0.064 | | |
| Coefficient of variation (COV)% | | | 3.2 | | | 4.3 | | | 5.9 | | |

*For specimens subjected to cyclic loading, stiffness was calculated at a lateral drift of 5.7%

### 2.7 Parametric Investigation

After the accuracy of the numerical model was verified, a parametric investigation was created to better understand the behavior of the CFST columns that were externally strengthened with FRP sheets and exposed to cyclic loading. The parametric study examined the impacts of the thickness, location, and effective length of the strengthening sheets on the lateral load–drift responses, initial stiffness, damping ratio, and absorbed energy of the CFST columns. The major goal of this study is to find the most economical FRP sheet design that will increase the structural capacity and energy absorption of the CFST columns exposed to cyclic loading. In order to achieve such an objective, 14 CFST columns with different FRP sheet thickness, location, and length were constructed and analyzed using the 3D numerical model. The samples were divided into three groups. The effect of the FRP thickness was studied in the first group, which changed to include one layer (0.167 mm), two layers, three layers, four layers, and five layers. In this group, the entire length of the CFST column has been strengthened.

The second group evaluated how the location of the strengthening sheets, whether they were at the top of the column at the loading zone, in the middle of the column, or at the bottom of the column at the fixed support, affected the capacity of the CFST columns. In this group, three FRP sheets with a total thickness of 0.501 mm were used to strengthen the half-length of the CFST columns. The decision to use three sheets to strengthen specimens of the second group was made in an effort to strike a balance between the increase in lateral capacity of CFST columns and the total cost that increases as the number of FRP layers increases. The third group addressed the impact of the length of FRP sheets on the lateral load and the pattern of failure of CFST columns. This group included five columns, all of which were strengthened with three layers of FRP sheets in the bottom region near the fixed support. The length of FRP sheets used in the study was 10, 20, 30, 40, and 70% of the total length of the CFST column (L). The behavior of the three groups will be compared to that of the control CFST column specimen that is not supported by FRP sheets (C-0-0). Table 5 displays the configurations and numerical results of the analyzed CFST columns. It is important to note that the current parametric investigation took into account the same loading and boundary conditions that Ji et al. (2023) had previously employed. The cyclic loading protocol was established utilizing displacement control criteria, and each displacement loading cycle was specified to consist of two cycles. The defined lateral drift was 0.3%, 0.6%, 0.8%, 1.15%, 1.70%, 2.3%, 3.5%, and 5.7%, as shown in Fig. 2.

### 2.8 Failure Pattern

When the control CFST column that was not supported by FRP sheets (C-0-0) was loaded to an approximate lateral drift of 1.7%, there was slight outward local buckling of the steel tube near the fixed support, where maximum stresses were concentrated. As the applied load increased up to lateral drift of 5.7%, the outward local buckling

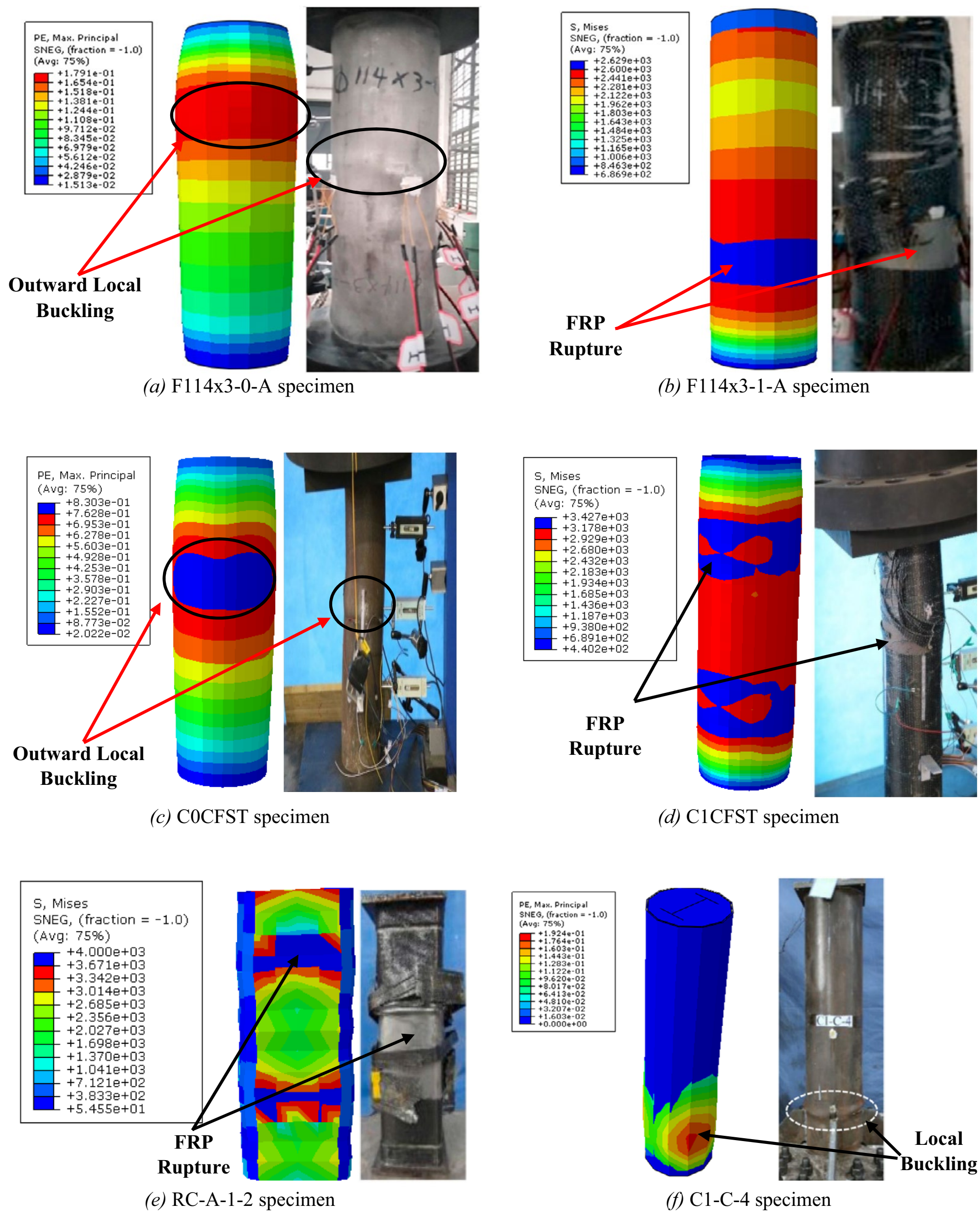


**Fig. 4** Experimental versus numerical failure patterns

became more obvious, as depicted in Fig. 6a. The failure patterns of the specimens within the first group demonstrate that FRP sheets, even when applied at low thickness, were effective at confining the steel tube and postponing the emergence of outward local buckling. For the two specimens in which the entire length of the CFST column was strengthened with one and two layers of FRP sheets, C-1-L and C-2-L, respectively, it was observed that the steel tube began to buckle at a lateral drift of 2.3% compared to 1.7% for the control column. Then, FRP sheets ruptured near the fixed support at a lateral drift of 5.7%. Also, with the increase in the number of FRP layers to three, four, and five layers (C-3-L, C-4-L, and C-5-L), the outward buckling of the steel tube was initiated at a lateral drift of 3.5%, while the rupture of the strengthening layers near the fixed support occurred at a lateral drift of 5.7%, as shown in Fig. 6b.

Before starting to study the impact of the effective length of the strengthening sheets on the behavior of the CFST columns exposed to cyclic loadings, it was

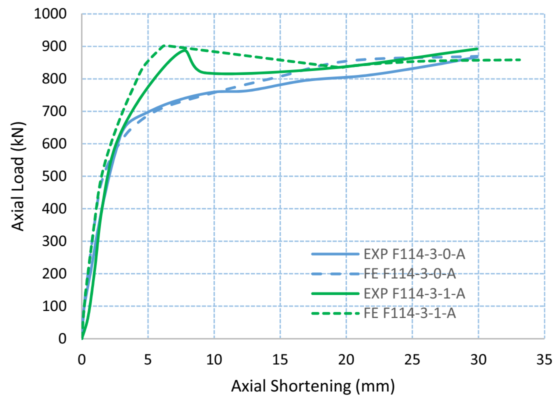


*(a)* Specimens tested by Tang et al. [52].

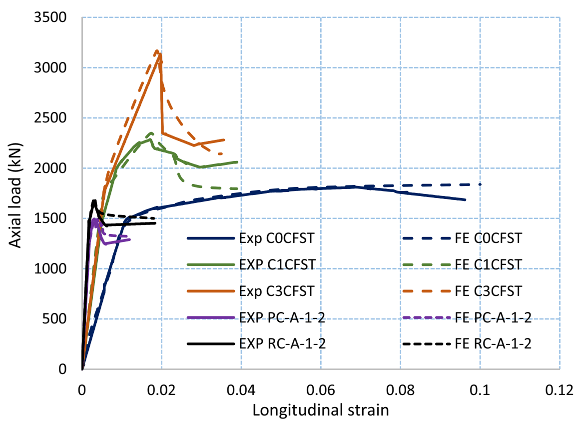


*(b)* Specimens tested by Wang et al. [20] and Zhang et al. [56].

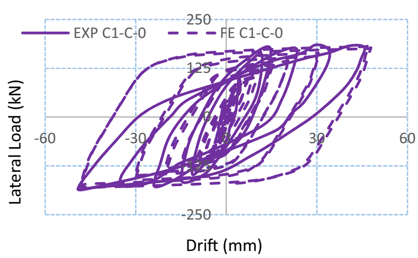


*(c) C1-C-0 specimen*

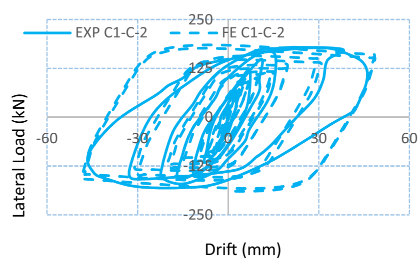


*(d) C1-C-2 specimen*

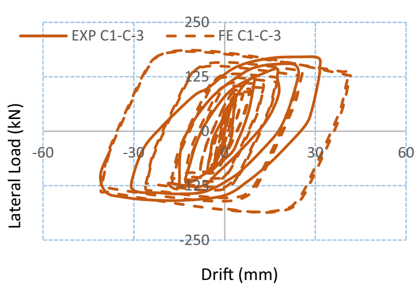


*(e) C1-C-3 specimen*

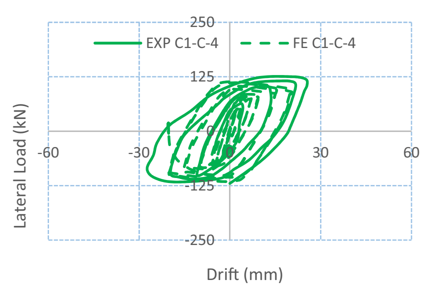


*(f) C1-C-4 specimen*

**Fig. 5** Experimental versus FE responses

**Table 5** Configurations and results of the parametric study

| Specimen ID | Diameter mm | Thickness mm | Length mm | FRP thickness mm | FRP length mm | FRP location | $P_{max}$ kN | % gain in $P_{max}$ | $\Delta_{max}$ mm | $K$ kN/mm | Absorbed energy kN.mm | Failure mode |
|---|---|---|---|---|---|---|---|---|---|---|---|---|
| C-0-0 | 220 | 4.0 | 900 | – | – | – | 185 | – | 49.1 | 16.4 | 94,000 | LB |
| C-1-L | 220 | 4.0 | 900 | 0.167 | 900 | Whole length | 209 | 13 | 48.8 | 24.28 | 103,238 | FRP-R |
| C-2-L | 220 | 4.0 | 900 | 0.334 | 900 | | 226 | 22 | 47.3 | 24.64 | 105,700 | FRP-R |
| C-3-L | 220 | 4.0 | 900 | 0.501 | 900 | | 245 | 32 | 49.0 | 24.68 | 107,840 | FRP-R |
| C-4-L | 220 | 4.0 | 900 | 0.668 | 900 | | 268 | 45 | 48.9 | 25.12 | 112,948 | FRP-R |
| C-5-L | 220 | 4.0 | 900 | 0.835 | 900 | | 277 | 50 | 47.9 | 25.5 | 117,340 | FRP-R |
| C-3-0.5LB | 220 | 4.0 | 900 | 0.501 | 450 | Bottom | 241 | 30 | 48.6 | 24.21 | 106,738 | FRP-R |
| C-3-0.5LM | 220 | 4.0 | 900 | 0.501 | 450 | Middle | 190 | 3.0 | 48.0 | 24.12 | 100,044 | LB |
| C-3-0.5LU | 220 | 4.0 | 900 | 0.501 | 450 | Upper | 187 | 1.0 | 47.5 | 24.12 | 95,240 | LB |
| C-3-0.1LB | 220 | 4.0 | 900 | 0.501 | 90 | Bottom | 197 | 6.0 | 47.0 | 23.28 | 99,552 | LB |
| C-3-0.2LB | 220 | 4.0 | 900 | 0.501 | 180 | Bottom | 209 | 13 | 48.8 | 23.94 | 103,238 | LB |
| C-3-0.3LB | 220 | 4.0 | 900 | 0.501 | 270 | Bottom | 225 | 22 | 48.1 | 24.10 | 105,246 | FRP-R |
| C-3-0.4LB | 220 | 4.0 | 900 | 0.501 | 360 | Bottom | 236 | 28 | 48.9 | 24.25 | 106,286 | FRP-R |
| C-3-0.7LB | 220 | 4.0 | 900 | 0.501 | 630 | Bottom | 244 | 32 | 48.5 | 24.56 | 107,126 | FRP-R |

$P_{max}$ maximum lateral load, $\Delta_{max}$ displacement at maximum lateral load, *K* initial stiffness, *LB* local buckling near fixed support, *FRP R* FRP rupture

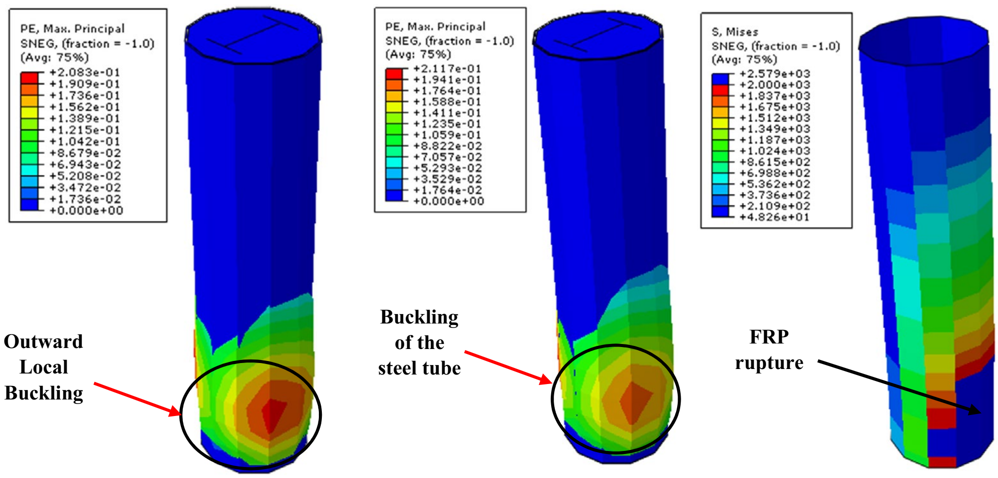


*(a)* C-0-0 specimen *(b)* C-4-L specimen

**Fig. 6** Failure patterns of the analyzed specimens

necessary to determine the optimal location for placing those FRP sheets, and herein lies the importance of the samples of the second group. In this group, the half-length of the CFST column was strengthened using three layers of FRP sheets at different locations, i.e., at the top of the column (C-3-0.5LU), in the middle of the column (C-3-0.5LM), or at the bottom of the column (C-3-0.5LB). Failure patterns of the analyzed three columns revealed that strengthening the CFST column at the bottom near the fixed support (C-3-0.5LB), where maximum stresses were concentrated, efficiently delayed the outward buckling of the steel tube. Accordingly, the specimen (C-3-0.5LB) was able to withstand a larger lateral load that ruptured the strengthening sheets at a lateral drift of 5.7%. The two other strengthening patterns failed to control the outward buckling of the steel tube due to the placement of FRP sheets outside the buckling zone, so the outward buckling occurred very early at a lateral drift of 1.7%. The effective length of FRP sheets at the bottom of the column around the stress concentration area near the fixed support was of interest to the third group. The use of FRP sheets at relatively short lengths of 10 and 20% (C-3-0.1LB and C-3-0.2LB) of the overall length of the CFST column was ineffective in preventing the steel tube's early outward buckling, which started at a lateral drift of 1.7%. The buckling was delayed to start at a 2.3% lateral drift followed with a rupture in the FRP sheets as the effective length of the strengthening sheets increased up to 30% and 40% (C-3-0.3LB and C-3-0.4LB) of the column length. When utilizing a strengthening length equal to half the length of the column (C-3-0.5LB), a similar failure pattern to the full-length strengthened specimen manifested, with the buckling appearing at a lateral drift of 3.7% and the cutting of the FRP sheets occurring at a drift of 5.7%. The development of the outward buckling or the FRP rupture with respect to the C-3-0.5LB specimen was unaffected by further extending the effective length of the FRP sheets, i.e., 70% of the column length (C-3-0.7LB).

### 2.9 Lateral Load–Drift Hysteresis Curves

Fig. 7 displays the lateral load–drift hysteresis curves of the three groups. Generally, the first group's findings demonstrate that altering the thickness of the strengthening sheets has a significant impact on the maximum lateral load of the CFST column. In comparison to columns strengthened with a smaller thickness, CFST columns strengthened with a greater thickness of FRP sheets demonstrated superior cyclic performance. At a lateral drift of 5.7%, the un-strengthened specimen C-0-0 demonstrated a maximum lateral load of 185 kN. Although the maximum lateral load of CFST columns was increased to 209 kN by using a single layer of 0.167 mm thick FRP sheet, the gain ratio over the control column was only 13%. The increased thickness of the FRP sheets increased the total resistant cross section area to cyclic loads and delayed the outward buckling of the steel tube. This resulted in an increase in the enhancement ratio of the maximum lateral load at the maximum lateral drift of 5.7% with respect to the control specimen. The gain in the maximum lateral load of specimens C-2-L, C-3-L, and C-4-L was 22, 32, and 45% compared to the C-0-0 CFST column. The highest lateral load of all examined columns was reached by specimen C-5-L, strengthened with the largest thickness of 0.835 mm (five layers), and it was also 50% greater than the control specimen.

Strengthening CFST columns outside the steel tube outward buckling zone cannot further improve the

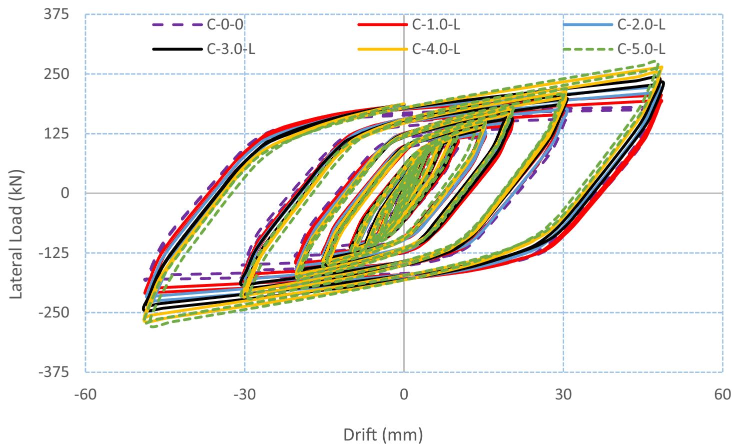


*(a)* Specimens of the first group

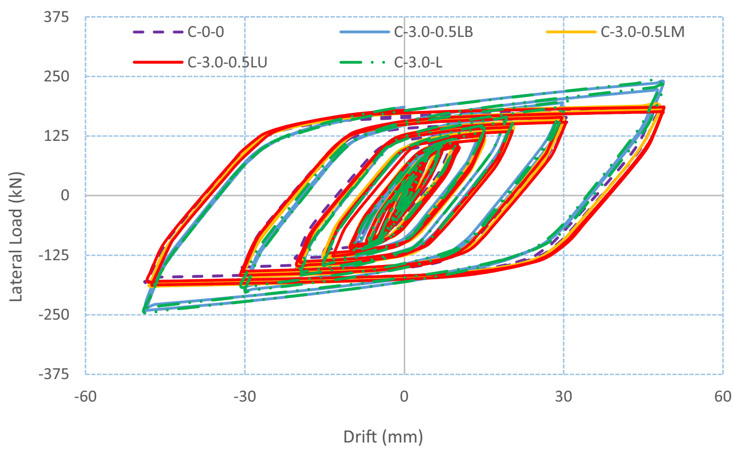


*(b)* Specimens of the second group

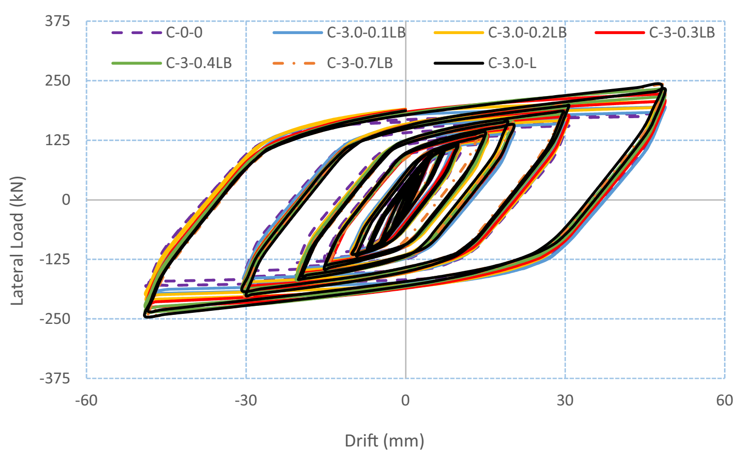


*(c)* Specimens of the third group

**Fig. 7** Hysteresis curves of the analyzed specimens maximum lateral load of examined specimens. A maximum lateral load of 190 kN was observed when FRP sheets were wrapped around the middle of the CFST column (C-3-0.5LM), while a smaller load of 187 kN was measured with strengthening the upper section of the CFST column (C-3-0.5LU). The increase in maximum lateral load of the C-3-0.5LM and C-3-0.5LU specimens over the control column C-0-0 was only 3% and 1%, respectively. The application of strengthening sheets with an adequate thickness of 0.501 mm (three layers) and an effective length of half the column's height at the bottom side (C-3-0.5LB) significantly postponed the buckling's initiation and limited its spread across the entire circular section. As a result, the C-3-0.5LB column's maximum lateral load was significantly enhanced; the measured gain over the control column was 30%. The results of the third group showed that the outward buckling of the steel tube could be controlled and delayed by increasing the effective length of FRP sheets in the maximum stress zone close to the fixed support. The shorter lengths of the strengthening sheets (10% and 20% of the total length of the column) enhanced the maximum lateral load at the maximum lateral drift of 5.7% due to the increased initial stiffness and the total cross-sectional area of the CFST column. However, the increase in the maximum lateral load was restricted to just 6% and 13% greater than the control column for C-3-0.1LB and C-3-0.2LB, respectively, since the shorter lengths of FRP sheets could not entirely cover the steel tube's buckling zone. As the effective length of the strengthening sheets increased, 30% and 40% of the whole length of the column, the buckling zone was totally confined. As a result, the spread of the outward buckling throughout the column cross section was delayed, and the maximum load increased significantly (22% and 28% above the control CFST column).

When the length of the strengthening sheets reached half the length of the CFST column, the recorded gain in the maximum lateral load was 30% compared to the control column. The improvement in the maximum lateral load reached 32% by extending the FRP sheets' length to 70% of the column's length, matching the gain ratio attained when the column's whole length was strengthened. In comparison to a strengthening length of 50% of the length of the column, the improvement ratio in the maximum lateral load while utilizing greater FRP lengths equal to 70% and 100% of the length of the column has not considerably improved. This is as a result of the steel tube's buckling zone being controlled and the spread of the outward buckling on its full circular section being delayed by strengthening it to a length that is equivalent to 50% of the column's length. The third group's findings show that, in order to balance the increase in the maximum lateral load of the CFST column with the overall cost, the usage of FRP sheets with a length equivalent to 50% of the length of the column can be regarded as the effective length of the strengthening sheets.

### 2.10 Absorbed Energy

The absorbed energy is a key parameter for evaluating the seismic performance of the composite members. In the current paper, the enclosed area of each cyclic loop was calculated and defined as the cumulative energy dissipation. The summation of cumulative energy dissipation at each cycle gives the absorbed energy value ($A_E$) of the specimen, as presented in Table 5. Fig. 8 displays the computed cumulative energy dissipation for all specimens in the three groups at each lateral drift level. Due to the CFST columns still being in the elastic zone, the results showed that when the drift was less than 1.70%, the energy dissipation among these specimens was roughly the same. As the applied lateral load increased, the energy dissipation increased, and a plastic deformation appeared at the bottom of the CFST columns, causing localized buckling of the steel tube or even rupture of the FRP sheets. Evidently, the results of the first group show that the thickness of the strengthening sheets significantly affects the cumulative energy dissipation, particularly at the plastic zone (between 5 and 48.6 mm). At the plastic zone, the CFST columns displayed obvious non-linear deformations, causing local buckling of the steel tube, which could be controlled using a higher thickness of strengthening layers. As a result, there would be a significant increase in the cumulative energy dissipation. At a lateral drift of 5.7%, the cumulative energy of the un-strengthened specimen C-0-0 was 24 kN m. Moreover, the cumulative energy of the strengthened columns (C-1-L, C-2-L, C-3-L, C-4-L, and C-5-L) was 26.1, 26.6, 27, 27.5, and 28 kN m., which was greater by 8, 10, 12, 13.5, and 15.2% compared to the C-0-0 CFST column, as presented in Fig. 8a.

By comparing the cumulative energy of specimens C-3-L and C-3-0.5LB, it was found that those two columns dissipated an almost similar amount of cumulative energy at each drift, as depicted in Fig. 8b. Additionally, as indicated in Table 5, the absorbed energy of specimens C-3-L and C-3-0.5LB was 107.8 and 106.7 kN m, respectively, 15% higher than the control specimen C-0-0. An absorbed energy of 100 kN m was observed when FRP sheets were wrapped around the middle of the CFST column (C-3-0.5LM). The smallest absorbed energy among the specimens of the second group, 95.2 kN.m, was obtained by strengthening the upper section of the CFST column (C-3-0.5LU). The increase in the absorbed energy of the C-3-0.5LM and C-3-0.5LU specimens over the control column C-0-0 was only 6.4% and 1.3%, respectively. This is mainly because the suggested strengthening

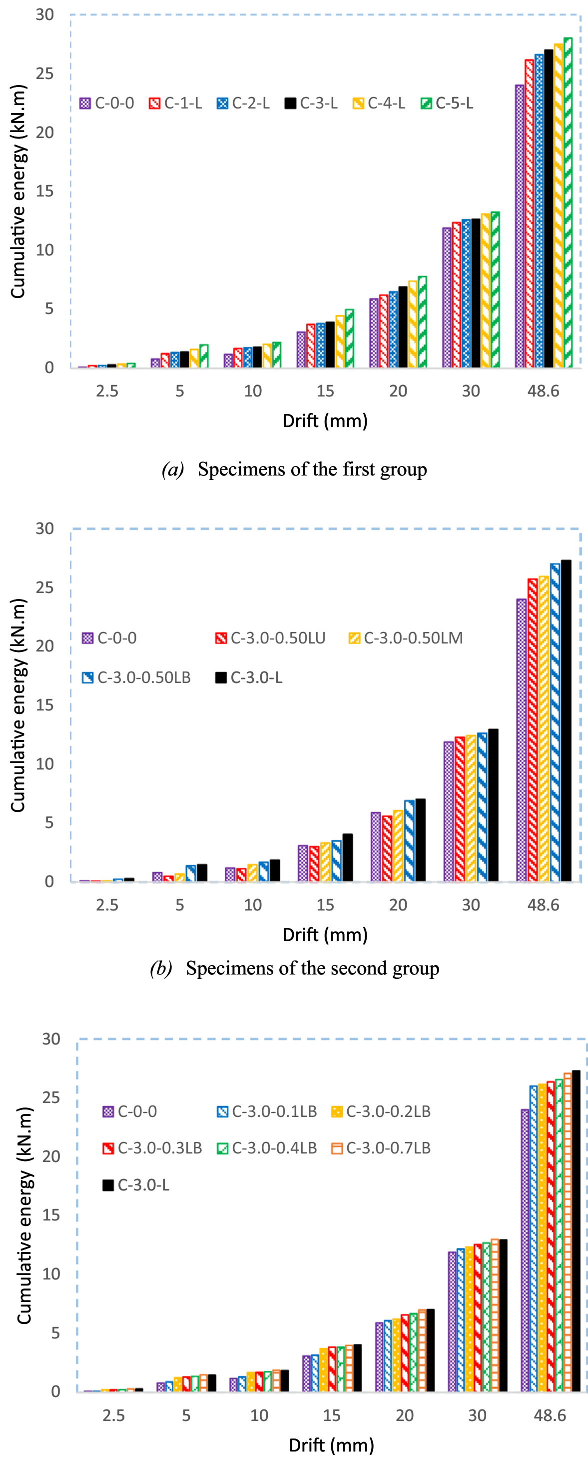


*(a)* Specimens of the first group

*(b)* Specimens of the second group

*(c)* Specimens of the third group

**Fig. 8** Cumulative energy dissipation of the analyzed specimens

techniques for such columns failed to prevent or even delay the outward buckling of the steel tube due to the placement of FRP sheets outside the buckling zone.

The third group's findings reveal that both cumulative and absorbed energy increased by increasing the effective length of FRP sheets in the maximum stress zone close to the fixed support, as indicated in Table 5 and Fig. 8c. This is principally due to the fact that the larger effective length of FRP sheets caused severe plastic deformation and delayed the outward buckling of the steel tube. In comparison with specimen C-3-0.5LB, the improvement ratio in the absorbed energy due to the strengthening of 70 and 100% (C-3-0.7LB and C-3-L) of the overall length of the CFST column has not been considerably improved. For example, the gain in the absorbed energy of specimens C-3-0.5LB and C-3-0.7LB was 13.6 and 14% greater than the control C-0-0 CFST column, very close to the gain ratio of specimen C-3-L (14.7%). At the maximum lateral drift of 5.7%, the FRP strengthening sheets, even if used with shorter lengths (10, 20, 30, and 40% of the total length of the column), effectively confined the CFST columns and delayed the outward buckling of the steel tube. Consequently, the cumulative energy was effectively enhanced with respect to the control column, as shown in Fig. 8c.

### 2.11 Envelop Curves and Initial Stiffness

The lateral load–drift envelope curves extracted from the hysteresis curves of all specimens are presented in Fig. 9. The response of all specimens generally remained practically linear when the drift ratio was less than 1.70% before becoming non-linear up until the completion of loading at a lateral drift of 5.70%. In addition, Table 5 displays the initial stiffness (K), which was calculated from the slope of the positive load–drift curves at a lateral drift of 0.3%, as illustrated in Eq. (13):

$$K = \frac{+P_{0.3}}{+\Delta_{0.3}}, \tag{13}$$

where $+P_{0.3}$ is the peak load at the first cycle and $+\Delta_{0.3}$ is the lateral drift corresponding to $P_{0.3}$.

When the initial stiffness values for the first group are compared, the initial stiffness of the FRP-strengthened CFST columns significantly exceeds that of the un-strengthened specimen. The initial stiffness of the un-strengthened specimen C-0-0 was 16.4 kN/mm. Moreover, the initial stiffness of the FRP-strengthened columns C-1-L, C-2-L, C-3-L, C-4-L, and C-5-L was 24.28, 24.64, 24.68, 25.12, and 25.5 kN/mm. It was confirmed that the gain in the initial stiffness of strengthened specimens with respect to the C-0-0 column was 48, 50.2, 50.5, 53.2, and 55.6% when one, two, three, four, and five FRP layers were used, respectively. This indicates a significant contribution of the FRP sheets to the initial stiffness of the CFST columns, as shown clearly in Fig. 9a.

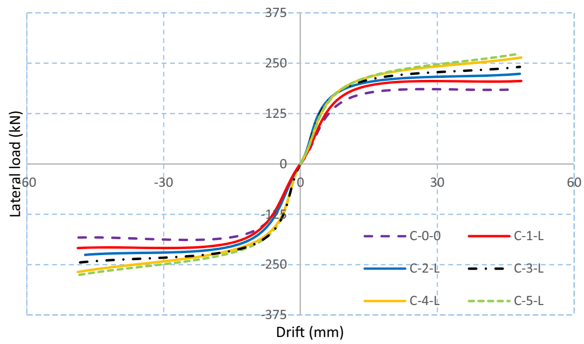


*(a)* Specimens of the first group

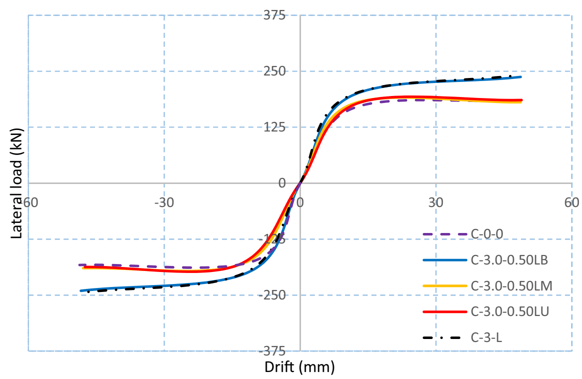


*(b)* Specimens of the second group

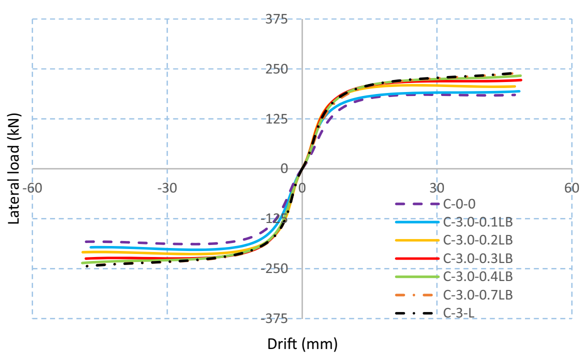


*(c)* Specimens of the third group

**Fig. 9** Envelop curves of the analyzed specimens

For specimens that were strengthened along half the length of the CFST column at different locations (C-3-0.5LM, C-3-0.5LU, and C-3-0.5LB), the improvement was 47.0, 47.0, and 47.6% compared with the un-strengthened specimen, respectively. It was found that the initial stiffness could be significantly improved by using strengthening sheets regardless of their location, as displayed in Fig. 9b, because at the elastic zone no plastic deformations leading to outward buckling were initiated.

The third group's findings indicate that the initial stiffness values gradually increased when the effective length of the strengthening sheets increased from 0.10 to 0.70L, as shown in Fig. 9c and Table 5. The gain in initial stiffness was significant, even with the use of shorter lengths of FRP sheets, as a result of the FRP's ability to confine the strengthened columns compared to the un-strengthened specimen. The initial stiffness of the CFST columns was increased by 42.0, 46.0, 47.0, 47.6, and 47.9%, respectively, over the C-0-0 specimen by strengthening the columns in the zone of maximum stress close to the fixed support with varied lengths of 10, 20, 30, 40, and 50% of the overall length of those columns. A slight improvement in the initial stiffness was noticed with regard to strengthening half the length of the column (C-3-0.5 LB) when the effective length of the strengthening sheets increased, representing 70 and 100% of the overall length of the CFST columns. The gain in initial stiffness of specimens C-3-0.7LB and C-3-L with respect to the C-0-0 column was 49.8 and 50.5%, respectively.

### 2.12 Viscous Damping Factor

In order to evaluate the seismic behavior of FRP-strengthened CFST columns, the equivalent viscous damping factor ($\xi_{eq}$) is calculated using Eq. (14) as previously recommended by Li et al. (2019); Yang et al., (2023); Javanmardi et al., (2020):

$$\xi_{eq} = \frac{S_{ABCDA}}{2\pi\left(S_{(\Delta OBE\,+\,\Delta ODF)}\right)}, \tag{14}$$

where $S_{ABCDA}$ is the area of the hysteretic loop of ABCD (the yellow area), and $S_{(\Delta OBE+\Delta ODF)}$ represents the total area of the two triangles ΔOBE and ΔOFD (the shadow area), as depicted in Fig. 10. Fig. 11a–c displays the damping factor $\xi_{eq}$-lateral drift curves for all specimens in the three groups at different drift levels. In general, for all 14 specimens, regardless of the strengthening configurations, the equivalent viscous damping factor increased as the drift ratio increased. In particular, it was seen by comparing the $\xi_{eq}$ values of several specimens within the first group in Fig. 11a that the $\xi_{eq}$ values steadily reduced as the FRP thickness raised from 0.167 mm to 0.835 mm. This is mostly due to the fact that higher lateral load was observed at the same lateral drift as FRP's thickness increased. Consequently, as shown in Fig. 10, the cumulative energy ($S_{ABCDA}$) of the FRP-strengthened CFST columns gradually increased, while the hatched regions ($S_{(\Delta OBE+\Delta ODF)}$) significantly enhanced in comparison to the control column. On the one hand, the control CFST column C-0-0 showed $\xi_{eq}$ of 45.2% at a lateral drift of 5.7%. On the other hand, at the same lateral drift the decrease in $\xi_{eq}$ values of FRP-strengthened CFST

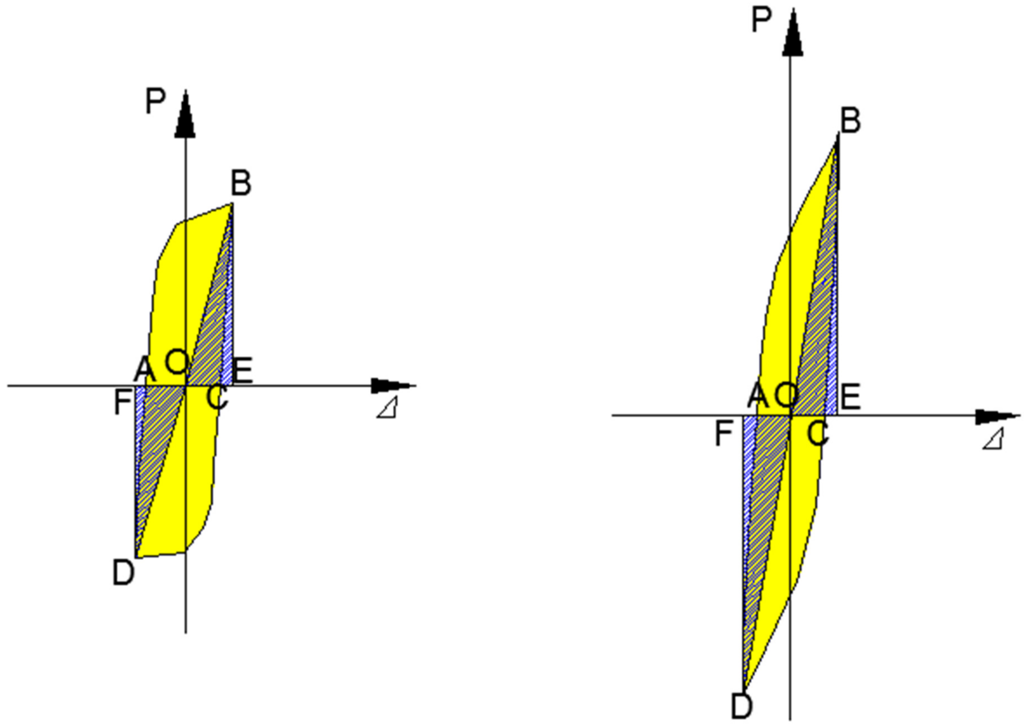


*(a)* Specimen C-0-0 *(b)* Specimen C-5-L

**Fig. 10** Definition of equivalent damping factor $\xi_{eq}$

specimens C-1-L, C-2-L, C-3-L, C-4-L, and C-5-L with respect to the control specimen was 7.9, 14.9, 20.8, 27.7, and 30.3%, respectively.

Fig. 11b reveals that $\xi_{eq}$ of specimens C-3-0.5LM and C-3-0.5LU at a lateral drift of 5.7% was 46.5 and 45.4%, respectively, which is quite similar to the control column. This pertains to the fact that the hysteresis response of the two samples C-3-0.5LM and C-3-0.5LU was identical to that of the C-0-0 column. Contrarily, the $\xi_{eq}$ of specimen C-3-0.5LB recorded a decrease at all levels of lateral drift compared to the C-3-0.5LM and C-3-0.5LU columns. At a lateral drift of 5.7%, the $\xi_{eq}$ of specimen C-3-0.5LB was 35.5%, which is 21.5% lower than the control CFST column.

The third group's findings indicate that the $\xi_{eq}$ values gradually decreased when the effective length of the FRP strengthening sheets increased from 0.1 to 0.5L due to enhancement of the hatched areas ($S_{(\Delta OBE+\Delta ODF)}$). At a lateral drift of 5.7%, the $\xi_{eq}$ values of specimens C-3-0.1LB, C-3-0.2LB, C-3-0.3LB, C-3-0.4LB, and C-3-0.5LB was 44.4, 42.6, 40.7, 38.6, and 35.5%, respectively. While increasing the length of the FRP sheets at the bottom of the CFST column, where the largest stresses were concentrated, the results of the columns' equivalent viscous damping factor were not significantly changed. The equivalent viscous damping values of specimens strengthened with 70 or even 100% of their entire length closely match the result of a column strengthened with half its length. The $\xi_{eq}$ of specimen C-3-0.7LB and C-3-L was 35.8% at a lateral drift of 5.7%. The obtained results of the $\xi_{eq}$ are consistent with the trend of energy absorption, initial stiffness, and hysteresis responses. The results of the parametric study indicated that full-length strengthening of CFST columns is the most effective among all proposed techniques. Furthermore, increasing the number of layers of FRP strengthening enhances the lateral load capacity of CFST columns before FRP rupture occurs.

## 3 Conclusions

The cyclic response of CFST columns externally strengthened with FRP sheets was numerically investigated. The constructed 3D non-linear FEM was successfully able to capture the failure patterns and load–strain responses of experimental results on FRP-strengthened CFST columns subjected to monotonic loadings. Moreover, the FEM was used to represent the behavior of CFST columns exposed to cyclic loadings, and the model results matched the experimental results available in the literature. The validated FEM was utilized to run a parametric

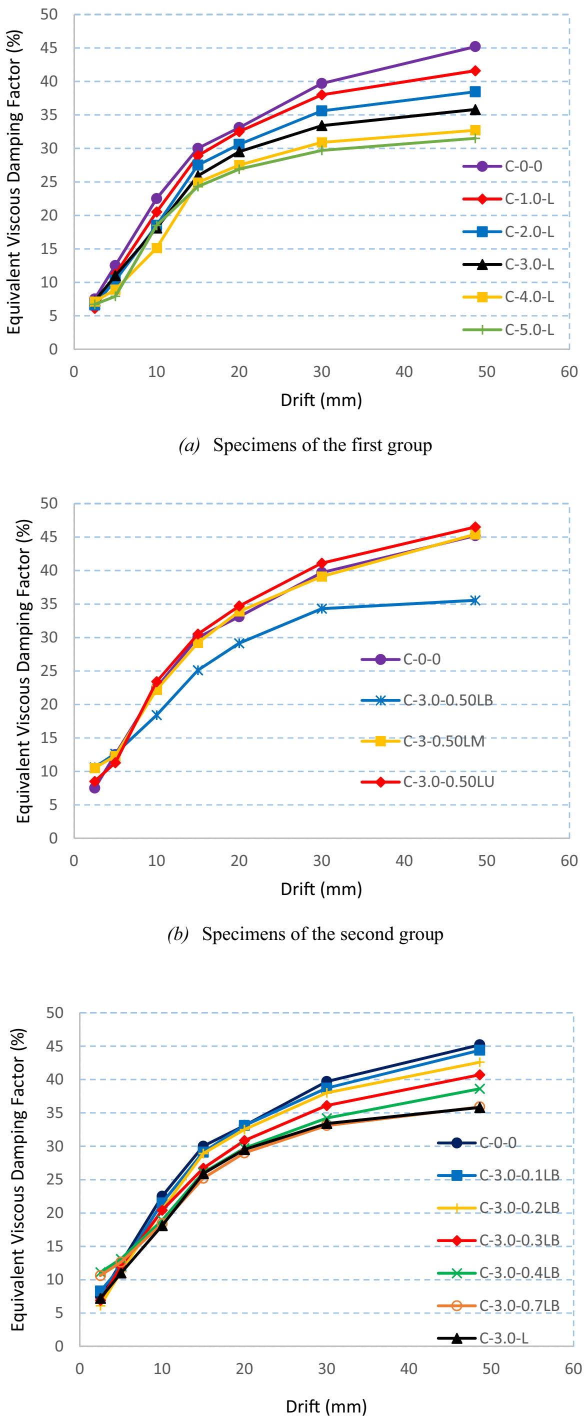


*(a)* Specimens of the first group

*(b)* Specimens of the second group

*(c)* Specimens of the third group

**Fig. 11** Equivalent viscous damping factor of the analyzed specimens

investigation in order to understand the response of FRP-strengthened CFST columns under cyclic loadings. The objective of the parametric study is to show the effects of FRP thickness, FRP location, and effective length of the FRP sheets on failure patterns, lateral load–drift responses, initial stiffness, cumulative energy, absorbed energy, and the viscous damping factor. The following conclusions were drawn:

1. FRP wrapping effectively confined the steel tube and postponed the emergence and propagation of outward local buckling even when applied at low thickness (0.167 and 0.334 mm), especially when located at the bottom of the column near the concentration of maximum stresses.
2. The results of the parametric study indicated that full-length strengthening of CFST columns is the most effective among all proposed techniques.
3. Increasing the number of layers of FRP strengthening enhances the lateral load capacity of CFST columns before FRP rupture occurs.
4. Specimen C-5-L achieved the highest lateral load among all investigated columns (50% more than the control specimen) due to wrapping the CFST column using five layers of FRP sheets.
5. The application of FRP sheets at relatively short lengths of 10 and 20% of the total length of the CFST column was ineffective in avoiding early outward buckling of the steel tube.
6. When strengthening half the length of the column, buckling appears at a lateral drift of 3.7%, and the FRP sheets are cut at a drift of 5.7%.
7. The un-strengthened specimen C-0-0 displayed a maximum lateral load of 185 kN at a lateral drift of 5.7%.
8. When the length of the strengthening sheets reached 30% of the whole length of the column, the buckling zone was totally confined. As a result, the maximum load significantly increased (22% higher than the control CFST column).
9. When the drift ratio was less than 1.70%, the envelope load–drift response of all specimens remained essentially linear before becoming non-linear up until the completion of loading at a lateral drift of 5.70%.
10. The cumulative energy of the C-0-0 specimen was 24 kN m at a lateral drift of 5.7%. Furthermore, the cumulative energy of the strengthened columns (C-1-L, C-2-L, C-3-L, C-4-L, and C-5-L) was 26.1, 26.6, 27, 27.5, and 28 kN m, respectively, 8%, 10%, 12%, 13.5%, and 15.2% greater than that of the C-0-0 CFST column.
11. At a lateral drift of 5.7%, the decrease in viscous damping factor of CFST specimens due to strengthening using 1, 2, 3, 4, and 5 layers of FRP sheets with respect to the control specimen was 7.9%, 14.9%, 20.8%, 27.7%, and 30.3%, respectively.

### 3.1 Limitations and future work

The limitation of the current study lies in the use of steel tubes of one thickness only, and the strengthening was mainly done using carbon fibers, as glass or aramid fibers were not extensively utilized in previous experimental studies. Accordingly, the following points represent necessary extensions of the current study:

1. Investigate the effect of steel tube thickness on the cyclic response of concrete-filled steel tubular columns externally strengthened with FRP composites.
2. Study the experimental behavior of concrete-filled steel tubular columns strengthened with glass fiber-reinforced polymers and aramid fiber-reinforced polymers.

**Acknowledgements**
The finite element modeling was carried out based on the co-operation between the Civil and Transportation College, Shenzhen University, China, and the Civil Engineering Department, Faculty of Engineering, Kafrelsheikh University, Egypt. The authors would like to appreciate the financial support provided by Shenzhen Science and Technology Innovation Committee (No. JCYJ20220531101415036 and 20220811100052001). Also, the authors would like to acknowledge the technical support provided by Guangdong Provincial Key Laboratory of Durability for Marine Civil Engineering (SZU) (No. 2020B1212060074).

**Author contributions**
Walid Mansour: conceptualization, methodology, idea of the research, writing, writing-review, supervision and editing. Bothaina Osama: conceptualization, methodology, idea of the research, writing, writing-review and editing. Weiwen Li: conceptualization, methodology, idea of the research, writing, writing-review, supervision and editing. Peng Wang: conceptualization, methodology, idea of the research, writing, and writing-review. Md. Habibur Rahman Sobuz: methodology, writing, writing-review, and editing.

**Funding**
The authors received no financial support for the research, authorship, and/or publication of this article.

**Availability of data and materials**
Some of all the data, models, or codes that support the findings of this study are available from the corresponding author upon reasonable request.

## Declarations

**Ethics approval and consent to participate**
None.

**Consent for publication**
None.

**Competing interests**
No potential conflict of interest was reported by the authors.

**Author details**
[1]Guangdong Provincial Key Laboratory of Durability for Marine Civil Engineering, Shenzhen University, Shenzhen 518060, China. [2]Civil Engineering Department, Faculty of Engineering, Kafrelsheikh University, Kafrelsheikh, Egypt. [3]Structural Engineer, Tanta, Egypt. [4]Department of Civil and Environmental Engineering, The Hong Kong University of Science and Technology, Hong Kong, China. [5]Department of Building Engineering and Construction Management, Khulna University of Engineering and Technology, Khulna 9203, Bangladesh.

Received: 7 December 2023 Accepted: 5 August 2024
Published online: 27 November 2024

**References**

ABAQUS. (2017). ABAQUS, Standard User's Manual, Version 6.17, Dassault Systemes SIMULIA Corp., Providence, RI (USA).

Abdal, S., Mansour, W., Agwa, I., Nasr, M., Abadel, A., Onuralp Özkılıç, Y., et al. (2023). Application of ultra-high-performance concrete in bridge engineering: current status, limitations, challenges, and future prospects. *Buildings, 13*, 185.

ACI. (2008). Building code requirements for structural concrete and commentary. ACI 318M-08. USA: American Concrete Institute.

Ahmed, M., Ci, J., Yan, X.-F., Lin, S., & Chen, S. (2021). Numerical modeling of axially loaded circular concrete-filled double-skin steel tubular short columns incorporating a new concrete confinement model. *Structures., 30*, 611–627.

Basha, A., Tayeh, B. A., Maglad, A. M., & Mansour, W. (2023). Feasibility of improving shear performance of RC pile caps using various internal reinforcement configurations: Tests and finite element modelling. *Engineering Structures., 289*, 116340.

Binici, B. (2005). An analytical model for stress–strain behavior of confined concrete. *Engineering Structures., 27*, 1040–1051.

Brown, N. K., Kowalsky, M. J., & Nau, J. M. (2015). Impact of D/t on seismic behavior of reinforced concrete filled steel tubes. *Journal of Constructional Steel Research., 107*, 111–123.

Chen, Z., Zhou, J., Jing, C., & Tan, Q. (2021). Mechanical behavior of spiral stirrup reinforced concrete filled square steel tubular columns under compression. *Engineering Structures., 226*, 111377.

Chin, C.-L., Ma, C.-K., Tan, J.-Y., Ong, C.-B., Awang, A. Z., & Omar, W. (2019). Review on development of external steel-confined concrete. *Construction and Building Materials., 211*, 919–931.

De Nicolo, B., Pani, L., & Pozzo, E. (1994). Strain of concrete at peak compressive stress for a wide range of compressive strengths. *Materials and Structures., 27*, 206–210.

Ding, F.-X., Fang, C., Bai, Y., & Gong, Y.-Z. (2014). Mechanical performance of stirrup-confined concrete-filled steel tubular stub columns under axial loading. *Journal of Constructional Steel Research., 98*, 146–157.

Ding, F.-X., Lu, D.-R., Bai, Y., Zhou, Q.-S., Ni, M., Yu, Z.-W., et al. (2016). Comparative study of square stirrup-confined concrete-filled steel tubular stub columns under axial loading. *Thin-Walled Structures., 98*, 443–453.

Dong, H., Qin, J., Cao, W., & Zhao, L. (2022). Seismic behavior of circular CFST columns with different internal constructions. *Engineering Structures., 260*, 114262.

Elchalakani, M., & Zhao, X.-L. (2008). Concrete-filled cold-formed circular steel tubes subjected to variable amplitude cyclic pure bending. *Engineering Structures., 30*, 287–299.

Elwakkad, N. Y., Heiza, K. M., & Mansour, W. (2023). Experimental study and finite element modelling of the torsional behavior of self-compacting reinforced concrete (SCRC) beams strengthened by GFRP. *Case Studies in Construction Materials., 18*, e02123.

Fang, S., Liu, F., Xiong, Z., Fang, J., & Li, L. (2019). Seismic performance of recycled aggregate concrete-filled glass fibre-reinforced polymer-steel composite tube columns. *Construction and Building Materials., 225*, 997–1010.

Han L-HJS, Beijing. Concrete filled steel tubular structures-theory and practice. 2007.

Han, L.-H., & Yang, Y.-F. (2005). Cyclic performance of concrete-filled steel CHS columns under flexural loading. *Journal of Constructional Steel Research., 61*, 423–452.

Hany, N. F., Hantouche, E. G., & Harajli, M. H. (2016). Finite element modeling of FRP-confined concrete using modified concrete damaged plasticity. *Engineering Structures., 125*, 1–14.

Hatzigeorgiou, G. D., & Beskos, D. E. (2005). Minimum cost design of fibre-reinforced concrete-filled steel tubular columns. *Journal of Constructional Steel Research., 61*, 167–182.

Hu, H.-S., Chen, Z.-X., Wang, H.-Z., & Guo, Z.-X. (2022). Seismic behavior of square spiral-confined high-strength concrete-filled steel tube columns under high axial load ratio. *Engineering Structures., 252*, 113600.

Hu, H., & Seracino, R. (2014). Analytical model for FRP-and-steel-confined circular concrete columns in compression. *Journal of Composites for Construction., 18*, A4013012.
Hu, H.-S., Tan, Y.-Y., Xu, L., Basha, S. H., & Ji, X.-R. (2024). High-strength concrete-filled steel tube columns with tie bars: Seismic behavior and design. *Journal of Constructional Steel Research., 212*, 108289.
Hu, H.-S., Wang, H.-Z., Guo, Z.-X., & Shahrooz, B. M. (2020). Axial compressive behavior of square spiral-confined high-strength concrete-filled steel-tube columns. *Journal of Structural Engineering., 146*, 04020136.
Javanmardi, A., Ghaedi, K., Ibrahim, Z., Huang, F., & Xu, P. J. (2020). Development of a new hexagonal honeycomb steel damper. *Archives of Civil and Mechanical Engineering., 20*, 1–19.
Ji, S.-H., Wang, W.-D., Xian, W., & Shi, Y.-L. (2023). Cyclic and monotonic behaviour of steel-reinforced concrete-filled steel tubular columns. *Thin-Walled Structures., 185*, 110644.
Li, C., Bi, K., Hao, H., Zhang, X., & Van Tin, D. (2019). Cyclic test and numerical study of precast segmental concrete columns with BFRP and TEED. *Bulletin of Earthquake Engineering., 17*, 3475–3494.
Li, G., Zhan, Z., Yang, Z., Fang, C., & Yang, Y. (2020). Behavior of concrete-filled square steel tubular stub columns stiffened with encased I-section CFRP profile under biaxial bending. *Journal of Constructional Steel Research., 169*, 106065.
Liu, J., Li, X., Zang, X., Chen, Y. F., & Wang, X. (2018). Hysteretic behavior and modified design of square TSRC columns with shear studs. *Thin-Walled Structures., 129*, 265–277.
Madenci, E., Fayed, S., Mansour, W., & Özkılıç, Y. O. (2022). Buckling performance of pultruded glass fiber reinforced polymer profiles infilled with waste steel fiber reinforced concrete under axial compression. *Steel and Composite Structures, an International Journal., 45*, 653–663.
Mansour, W., & Fayed, S. (2021). Flexural rigidity and ductility of RC beams reinforced with steel and recycled plastic fibers. *Steel and Composite Structures, an International Journal., 41*, 317–334.
Mansour, W., Li, W., Wang, P., & Badawi, M. (2024). Experimental and numerical evaluations of the shear performance of recycled aggregate RC beams strengthened using CFRP sheets. *Engineering Structures., 301*, 117368.
Mansour, W., Tayeh, B. A., & Tam, L.-H. (2022). Finite element analysis of shear performance of UHPFRC-encased steel composite beams: Parametric study. *Engineering Structures., 271*, 114940.
Patel, V. I., Liang, Q. Q., & Hadi, M. N. S. (2014). Numerical analysis of high-strength concrete-filled steel tubular slender beam-columns under cyclic loading. *Journal of Constructional Steel Research., 92*, 183–194.
Qian, J., Li, N., Ji, X., & Zhao, Z. (2014). Experimental study on the seismic behavior of high strength concrete filled double-tube columns. *Earthquake Engineering and Engineering Vibration., 13*, 47–57.
Samani, A. K., & Attard, M. M. (2012). A stress–strain model for uniaxial and confined concrete under compression. *Engineering Structures., 41*, 335–349.
Serras, D. N., Skalomenos, K. A., Hatzigeorgiou, G. D., & Beskos, D. E. (2016). Modeling of circular concrete-filled steel tubes subjected to cyclic lateral loading. *Structures., 8*, 75–93.
Sharif, A. M., Al-Mekhlafi, G. M., & Al-Osta, M. A. (2019). Structural performance of CFRP-strengthened concrete-filled stainless steel tubular short columns. *Engineering Structures., 183*, 94–109.
Shi, Y., Swait, T., & Soutis, C. (2012). Modelling damage evolution in composite laminates subjected to low velocity impact. *Composite Structures., 94*, 2902–2913.
Skalomenos, K. A., Hatzigeorgiou, G. D., & Beskos, D. E. (2014). Parameter identification of three hysteretic models for the simulation of the response of CFT columns to cyclic loading. *Engineering Structures., 61*, 44–60.
Tam, L.-H., Minkeng, M. A. N., Lau, D., Mansour, W., & Wu, C. (2023). Molecular interfacial shearing creep behavior of carbon fiber/epoxy matrix interface under moisture condition. *Engineering Fracture Mechanics., 282*, 109177.
Tang, H., Chen, J., Fan, L., Sun, X., & Peng, C. (2020). Experimental investigation of FRP-confined concrete-filled stainless steel tube stub columns under axial compression. *Thin-Walled Structures., 146*, 106483.
Tao, Z., Uy, B., Liao, F.-Y., & Han, L.-H. (2011). Nonlinear analysis of concrete-filled square stainless steel stub columns under axial compression. *Journal of Constructional Steel Research., 67*, 1719–1732.
Tao, Z., Wang, Z.-B., & Yu, Q. (2013). Finite element modelling of concrete-filled steel stub columns under axial compression. *Journal of Constructional Steel Research., 89*, 121–131.
Van Cao, V., Vo, C. T., Nguyen, P. T., & Ashraf, M. (2021). Experimental behaviour of circular concrete filled steel tube columns under lateral cyclic loading. *Earthquakes and Structures., 21*, 445–460.
Varma, A. H., Ricles, J. M., Sause, R., & Lu, L.-W. (2002). Seismic behavior and modeling of high-strength composite concrete-filled steel tube (CFT) beam–columns. *Journal of Constructional Steel Research., 58*, 725–758.
Wang, F.-C., Xie, W.-Q., Li, B., & Han, L.-H. (2022). Experimental study and design of bond behavior in concrete-filled steel tubes (CFST). *Engineering Structures., 268*, 114750.
Wang, J., Li, J.-R., Li, H., & Lv, L.-Y. (2023). Behaviour of square concrete-filled steel tubes reinforced with internal latticed steel angles under bending. *Structures., 48*, 1436–1454.
Wang, Q., Zhao, D., & Guan, P. (2004). Experimental study on the strength and ductility of steel tubular columns filled with steel-reinforced concrete. *Engineering Structures., 26*, 907–915.
Wang, Y., Cai, G., Si Larbi, A., Waldmann, D., Daniel Tsavdaridis, K., & Ran, J. (2020). Monotonic axial compressive behaviour and confinement mechanism of square CFRP-steel tube confined concrete. *Engineering Structures., 217*, 110802.
Xu, L., Hu, H.-S., Peng, B., & Guo, Z.-X. (2023). Seismic performance of composite jacket-confined square high-strength concrete-filled steel tube columns. *Journal of Constructional Steel Research., 211*, 108128.
Xu, T., Liu, J., Wang, X., Guo, Y., & Chen, Y. F. (2020). Behaviour of short CFRP-steel composite tubed reinforced normal and high strength concrete columns under eccentric compression. *Engineering Structures., 205*, 110096.
Yang, Z.-M., Chen, J., Wang, F., & Wang, J. (2023). Seismic performance of circular concrete-filled steel tube columns reinforced with inner latticed steel angles. *Journal of Constructional Steel Research., 205*, 107908.
Yu, T., Hu, Y. M., & Teng, J. G. (2014). FRP-confined circular concrete-filled steel tubular columns under cyclic axial compression. *Journal of Constructional Steel Research., 94*, 33–48.
Yuan, F., Cao, L., & Li, H. (2022). Axial compressive behaviour of high-strength steel spiral-confined square concrete-filled steel tubular columns. *Journal of Constructional Steel Research., 192*, 107245.
Yuan, F., Chen, M., Huang, H., Xie, L., & Wang, C. (2018). Circular concrete filled steel tubular (CFST) columns under cyclic load and acid rain attack: Test simulation. *Thin-Walled Structures., 122*, 90–101.
Zhang, S., Miao, K., Wei, Y., Xu, X., Luo, B., & Shi, W. (2023). Experimental and theoretical study of concrete-filled steel tube columns strengthened by FRP/steel strips under axial compression. *International Journal of Concrete Structures and Materials., 17*, 1.
Zhou, X., & Liu, J. (2010). Seismic behavior and strength of tubed steel reinforced concrete (SRC) short columns. *Journal of Constructional Steel Research., 66*, 885–896.

## Publisher's Note



**Walid Mansour** Postdoctor fellow, Civil and Transportation Engineering Department, Shenzhen University, Shenzhen 518,060, China. Associate Professor, Civil Engineering Department, Faculty of Engineering, Kafrelsheikh University, Kafrelsheikh, Egypt.

**Bothaina Osama** Structural Engineer, Tanta, Egypt.

**Weiwen Li** Professor, Civil and Transportation Engineering Department, Shenzhen University, Shenzhen 518060, China.

**Peng Wang** Assistant Professor, Civil and Transportation Engineering Department, Shenzhen University, Shenzhen 518060, China. Assistant Professor, Department of Civil and Environmental Engineering, The Hong Kong University of Science and Technology, Hong Kong, China.

**Md. Habibur Rahman Sobuz** Assistant Professor, Department of Building Engineering and Construction Management, Khulna University of Engineering & Technology, Khulna 9203, Bangladesh.